

Adaptive Feedback Guidance for Small-Body Landings with Generalized ZEM/ZEV and Nonlinear Optimization

Giovanni Fereoli*

Abstract—Precision landing on both large and small planetary bodies is a critical technology for advancing future human and robotic exploration of the solar system. Among the various approaches, the Zero-Effort-Miss/Zero-Effort-Velocity (ZEM/ZEV) feedback guidance algorithm has been extensively studied and remains a subject of active research. Despite its strengths in terms of accuracy and simplicity, the algorithm exhibits certain limitations. In this paper, it is proposed an adaptive guidance algorithm that builds upon the classical ZEM/ZEV framework by incorporating Constrained Nonlinear Optimization to address these limitations. This results in a closed-loop guidance algorithm that is lightweight for onboard spacecraft implementation and adaptable to various constraint scenarios. The proposed approach employs a Sequential Quadratic Programming (SQP) methodology to dynamically adjust the parameters of the guidance architecture based on the specific problem constraints.

Index Terms—Small-body landings, Soft-landing guidance, ZEM/ZEV algorithm, Nonlinear constraint optimization, Sequential Quadratic Programming

I. INTRODUCTION

A STEROID exploration has garnered significant scientific and public interest in recent years due to its multi-disciplinary importance. Motivations range from planetary defense and resource mining to studying asteroids as pristine archives of the Solar System's formation [1, 2, 3]. Among these, understanding surface and sub-surface properties is especially critical for unraveling their composition and evolutionary history [4, 5]. Spacecraft landings on asteroids significantly enhance scientific returns by enabling both in situ measurements and sample-return (SR) missions. Notable examples include JAXA's Hayabusa2 mission to Ryugu and NASA's OSIRIS-REx mission [6] to Bennu, both of which successfully performed precision landings.

Historically, missions such as Hayabusa [7] and Hayabusa2 [8] relied on sophisticated Guidance, Navigation, and Control (GNC) systems with closed-loop algorithms to manage trajectory control. These systems employed distinct control laws tailored to different descent phases, transitioning as needed during the maneuver. Alternatively, OSIRIS-REx utilized autonomously updated discrete maneuvers at specific checkpoints to construct its proximity operations trajectory. In contrast, ESA's Rosetta mission to comet 67P/Churyumov–Gerasimenko adopted a simpler approach for

*Graduate Research Assistant, Ann and H.J. Smead Department of Aerospace Engineering Sciences, University of Colorado, Boulder, 431 UCB, Colorado Center for Astrodynamics Research, Boulder, CO, 80309. AAS Member, AIAA Member.

its Philae lander, using a ballistic descent after precise injection [9]. To ensure a soft landing, Philae was equipped with anchoring harpoons and a cold gas retrothruster, illustrating the trade-offs between control complexity and hardware solutions.

Despite these successes, spacecraft autonomy in GNC remains constrained by operational limitations. Advancements in onboard decision-making are gradually addressing these challenges; however, there is still a strong need for robust, reliable, and computationally efficient algorithms to enable autonomous guided descent.

Powered descent trajectories for asteroid landings can be framed within the broader context of interception GNC [10], where the problem is modeled as the interception of a moving target. Typically, these missions employ continuous-thrust control algorithms, either as closed-loop systems that rely on in-flight measurements to refine commands or as open-loop systems with precomputed thrust profiles. Closed-loop systems remain the preferred approach for addressing state and dynamical uncertainties, particularly in autonomous operations.

Recent research has focused on robust control methods like Sliding Mode Control (SMC) have been investigated to tackle dynamical uncertainties. Notable examples include the Optimal Sliding Guidance (OSG) [11] and Multiple Surface Sliding Guidance algorithms, which augment traditional optimal guidance laws with robustness against perturbations. SMC methods have shown success, as demonstrated during Hayabusa2's landing phase [8]. Efforts have also been made to transform fuel-optimal constrained landing problems into convex optimization problems [12], enabling global solutions in polynomial time. Conversely, indirect methods based on Pontryagin's Minimum Principle (PMP) solve Two-Point Boundary Value Problems (TPBVPs) arising from optimality conditions. These methods, exemplified by Universal Powered Guidance (UPG) [13], offer flexibility but face challenges in enforcing inequality constraints and thrust direction limitations.

The ZEM/ZEV feedback guidance law [14], an analytical and straightforward application of optimal control theory, is particularly attractive for powered descent. It generates closed-loop acceleration commands that minimize energy (i.e., the integral of the square of acceleration). Although effective and simple, classical ZEM/ZEV struggles to enforce constraints such as thrust limits or glide-slope requirements. Attempts to address these limitations using intermediate waypoints [15] have shown promise but lack flexibility and real-time

adaptability.

This work introduces an enhanced ZEM/ZEV-based guidance algorithm for powered descent landing. The proposed approach adaptively adjusts both guidance gains and time-to-go at each time step to generate quasi-optimal closed-loop trajectories. These trajectories are fuel-efficient and meet critical flight constraints such as thrust limits and glide slope requirements. The algorithm leverages nonlinear optimization techniques, specifically Sequential Quadratic Programming (SQP) [16], to determine optimal guidance gains while preserving the simplicity of the ZEM/ZEV structure. By incorporating a nonlinear optimizer within the guidance loop, the method enables real-time enforcement of constraints while maintaining energy minimization and terminal accuracy. This approach retains the explainability and parametric simplicity of ZEM/ZEV guidance while significantly expanding its applicability to a wide range of environments and constraints. Future research will focus on optimizing the computational efficiency of the nonlinear optimizer to enable practical implementation for onboard autonomous descent. Addressing these challenges bridges the gap between the simplicity of classical ZEM/ZEV and the advanced capabilities of modern optimization techniques, providing a robust framework for future asteroid exploration missions.

II. THEORETICAL BACKGROUND

A. Dynamical Model

The motion of a spacecraft around an asteroid is analyzed in the asteroid's body-fixed reference frame, $\mathcal{B}_A = \{\hat{x}, \hat{y}, \hat{z}\}$. This frame is centered at the asteroid's center of mass and rotates with it, making it particularly suited for studying the spacecraft's dynamics during the final stages of proximity operations. At this stage, Coriolis and centripetal accelerations due to the asteroid's rotation must be explicitly included in the equations of motion. The axes of the reference frame are defined as follows: \hat{x} is aligned with the asteroid's axis of minimum moment of inertia, \hat{z} points along the principal axis of maximum inertia, and \hat{y} completes the right-handed orthogonal basis. These axes are typically derived from the asteroid's shape model. The state vector of the spacecraft in this frame is expressed as:

$$\mathbf{x} = [x, y, z, \dot{x}, \dot{y}, \dot{z}]^T = [\mathbf{r}, \mathbf{v}]^T$$

where x, y, z represent the spacecraft's position coordinates, and $\dot{x}, \dot{y}, \dot{z}$ denote the velocity components in the asteroid's body-fixed frame. The equations of motion governing the spacecraft's dynamics [17] are:

$$\ddot{\mathbf{r}} + 2\boldsymbol{\omega} \times \dot{\mathbf{r}} + \boldsymbol{\omega}^2 \hat{\mathbf{z}} \times (\hat{\mathbf{z}} \times \mathbf{r}) = -\nabla \Phi(\mathbf{r}) + \mathbf{u} \quad (1)$$

where $\boldsymbol{\omega}$ is the asteroid's rotational angular velocity, \mathbf{u} is control acceleration provided by the spacecraft's thrusters during powered descent, and Φ is the gravitational potential of the asteroid. The gravitational potential Φ is generally expressed as:

$$\Phi(\mathbf{r}) = G \int_V \frac{\rho(\mathbf{r}')}{|\mathbf{r} - \mathbf{r}'|} dV'$$

where G is the gravitational constant, $\rho(\mathbf{r}')$ is the asteroid's density at location \mathbf{r}' , and V is the volume of the asteroid. For simplicity, in this study, the asteroid's gravity is approximated as a point-mass potential:

$$\Phi(\mathbf{r}) = -\frac{\mu}{r}$$

where $\mu = GM$ represents the asteroid's gravitational parameter, with M being its mass. Perturbations such as solar radiation pressure (SRP) are neglected to focus on the fundamental dynamics. Future work may incorporate these effects for a more comprehensive analysis.

B. Guidance ZEM/ZEV Algorithm

Consider the problem of landing on a small-body of interest, with the mission spanning from time t_0 to t_f . The energy-optimal guidance problem can be formulated finding the acceleration \mathbf{u} that minimizes the performance index:

$$J = \frac{1}{2} \int_{t_0}^{t_f} \mathbf{u}^T \mathbf{u} dt \quad (2)$$

for a spacecraft subjected to the general dynamic equations of Equation 1. For simplicity, the acceleration contributions from gravity, Coriolis, and centrifugal effects are collectively represented as $\mathbf{f}(t)$. The boundary conditions are specified as:

$$\mathbf{r}(t_0) = \mathbf{r}_0, \quad \mathbf{r}(t_f) = \mathbf{r}_f^* \quad (3)$$

$$\mathbf{v}(t_0) = \mathbf{v}_0, \quad \mathbf{v}(t_f) = \mathbf{v}_f^* \quad (4)$$

No path constraints on the acceleration or spacecraft state are assumed. The necessary conditions can be derived via the Pontryagin Maximum Principle (PMP). The Hamiltonian for this problem is defined as:

$$H = \frac{1}{2} \mathbf{u}^T \mathbf{u} + \mathbf{p}_r^T \mathbf{v} + \mathbf{p}_v^T (\mathbf{f} + \mathbf{u}) \quad (5)$$

where \mathbf{p}_r and \mathbf{p}_v are the costate vectors associated with position and velocity, respectively. The time-to-go is defined as $t_{go} = t_f - t$. Applying the optimality condition yields the optimal acceleration:

$$\mathbf{u} = -t_{go} \mathbf{p}_r(t_f) - \mathbf{p}_v(t_f) \quad (6)$$

Substituting this expression into the dynamics equations allows solving for $\mathbf{p}_r(t_f)$ and $\mathbf{p}_v(t_f)$, resulting in the optimal control solution:

$$\begin{aligned} \mathbf{u} = & \frac{6}{t_{go}^2} [\mathbf{r}_f - (\mathbf{r} + t_{go} \mathbf{v})] \\ & - \frac{2}{t_{go}} [\mathbf{v}_f - \mathbf{v}] \\ & + \frac{6}{t_{go}^2} \int_t^{t_f} (\tau - t) \mathbf{f}(\tau) d\tau \\ & - \frac{4}{t_{go}} \int_t^{t_f} \mathbf{f}(\tau) d\tau. \end{aligned} \quad (7)$$

The Zero-Effort-Miss (ZEM) and Zero-Effort-Velocity (ZEV) are defined as the differences between the desired final position/velocity and the projected final position/velocity if no

additional control is applied:

$$\text{ZEM} = \mathbf{r}_f - \mathbf{r} - t_{go}\mathbf{v} - \int_t^{t_f} (t_f - \tau)\mathbf{f}(\tau) d\tau \quad (8)$$

$$\text{ZEV} = \mathbf{v}_f - \mathbf{v} - \int_t^{t_f} \mathbf{f}(\tau) d\tau \quad (9)$$

Substituting these definitions into the optimal control law yields [14]:

$$\mathbf{u} = \frac{6}{t_{go}^2} \text{ZEM} - \frac{2}{t_{go}} \text{ZEV} \quad (10)$$

In cases where \mathbf{f} is neither constant nor time-dependent, the control law is still usable but may no longer be optimal. For non-linear equations of motion or environments where the above assumptions do not hold, ZEM and ZEV must be computed numerically by integrating the equations of motion without control actions:

$$\text{ZEM} = \mathbf{r}_f - \mathbf{r}_{nc}, \quad (11)$$

$$\text{ZEV} = \mathbf{v}_f - \mathbf{v}_{nc}, \quad (12)$$

where \mathbf{r}_{nc} and \mathbf{v}_{nc} are the position and velocity at the mission's end without control.

III. ADAPTIVE GENERALIZED ZEM/ZEV GUIDANCE ALGORITHM

The classical ZEM/ZEV algorithm is widely recognized for its simplicity and effectiveness across diverse scenarios. However, while the classical ZEM/ZEV formulation guarantees valid trajectories in generalized environments, it loses its energy-optimality under such conditions. Moreover, it does not account for path constraints, such as thrust limits or glide-slope requirements. These limitations drive the development of the adaptive Generalized-ZEM/ZEV algorithm, expressed as:

$$\mathbf{u} = \frac{6k_r}{t_{go}^2} \text{ZEM} - \frac{2k_v}{t_{go}} \text{ZEV} \quad (13)$$

where constrained nonlinear optimization is employed to iteratively update specific guidance parameters in a closed-loop manner along the trajectory. The algorithm introduces the following adaptive elements:

- Gain parameters k_r and k_v , which scale the contributions of ZEM and ZEV in the commanded acceleration.
- Time-to-go (t_{go}), iteratively refined to achieve accurate terminal conditions while adhering to dynamic and physical constraints.

The approach of employing an optimizer to update the ZEM/ZEV parameters proves significantly more efficient than traditional nonlinear trajectory optimization methods, particularly direct methods. Unlike approaches that reformulate the guidance law using polynomials or other functional representations—often requiring the problem to be divided into numerous small segments, thereby increasing the dimensionality of the decision variables—this method maintains simplicity and avoids the computational burden associated with high-dimensional optimization.

1) Algorithm Implementation: As mentioned, the updates occur at each guidance cycle by exploiting a nonlinear optimizer. To preserve the energy-optimality of the original ZEM/ZEV algorithm and avoid suboptimal solutions in generalized dynamics, the algorithm minimizes a cost function based on the total commanded acceleration:

$$\min_{k_r, k_v, t_f} J = \frac{1}{2} \int_0^{t_{go}} \mathbf{u}^T \mathbf{u} dt$$

subject to the following constraints in addition to the spacecraft dynamics:

- 1) **Maximum thrust constraint:** The commanded acceleration must not exceed the spacecraft's thrust-to-weight capability:

$$\|\mathbf{u}\| \leq u_{\max}$$

- 2) **Glide-slope constraint:** The spacecraft's trajectory must remain within a specified glide-slope envelope, defined as:

$$r_{\perp} - \tan(\theta_{\text{glide}}) \cdot r_{\parallel} \leq 0$$

where $r_{\perp} = \sqrt{x_{rel}^2 + y_{rel}^2}$ and $r_{\parallel} = z_{rel}$. These are the perpendicular and parallel distances relative to the target state on the asteroid surface, with $\mathbf{r}_{rel} = \mathbf{r} - \mathbf{r}_f^*$.

- 3) **Terminal conditions:** The spacecraft must achieve the desired final position and velocity, as consistent with the original ZEM/ZEV formulation:

$$\mathbf{r}(t_f) = \mathbf{r}_f^*, \quad \mathbf{v}(t_f) = \mathbf{v}_f^*$$

The adaptive guidance algorithm is outlined in Algorithm 1. At each guidance cycle, the algorithm receives the current position \mathbf{r}_i and velocity \mathbf{v}_i as inputs. It then outputs the commanded acceleration \mathbf{u}_i for the current time step, alongside optimized parameters. To evaluate the cost function and ensure satisfaction of path constraints, the optimizer integrates the spacecraft dynamics and performs a simulation under the hood. However, to improve computational efficiency, an additional integration step to compute ZEM and ZEV after optimization is avoided. Instead, these quantities are approximated using a forward Euler step of size t_{go} , where the uncontrolled dynamics (with \mathbf{f}_i) are evaluated at the current time step. As shown in [14] for asteroid proximity operations, this approximation is valid because the uncontrolled acceleration \mathbf{f}_i is typically very small and can often be neglected without significant impact on the solution.

A. Problem Formulation and Parameters

This study addresses the problem of achieving a soft landing of a spacecraft on the surface of the small body 25143 Itokawa. The goal is to develop a guidance algorithm that ensures precise landing while satisfying physical constraints such as maximum thrust and glide-slope requirements. The small body's characteristics are defined by its gravitational and rotational properties: the gravitational parameter $\mu = 2.36 \times 10^{-9} \text{ km}^3/\text{s}^2$ and the rotational angular velocity $\boldsymbol{\omega} = [0 \ 0 \ 1.439 \times 10^{-4}]^T \text{ rad/s}$.

Algorithm 1 Adaptive ZEM/ZEV Guidance Algorithm

Require: $\mathbf{r}_i, \mathbf{v}_i, \mathbf{r}_f^*, \mathbf{v}_f^*, t_{i,go}, u_{\max}, \theta_{\text{glide}}$

Ensure: $k_r, k_v, t_{go}, \mathbf{u}$

- 1: Initialize parameters: $k_r \leftarrow 1, k_v \leftarrow 1, t_f \leftarrow t_{i,go}$
- 2: Configure settings for the nonlinear programming (NLP) solver.
- 3: Optimize k_r, k_v, t_f by solving the following NLP problem:

$$\min_{k_r, k_v, t_f} J = \int_0^{t_{go}} \mathbf{u}^T \mathbf{u} dt$$

subject to:

- Spacecraft Dynamics: $\ddot{\mathbf{r}} = \mathbf{f} + \mathbf{u}$, with \mathbf{u} derived from Equation 13.
- Thrust limit: $\|\mathbf{u}\| \leq u_{\max}$
- Glide-slope constraint: $r_{\perp} - \tan(\theta_{\text{glide}}) \cdot r_{\parallel} \leq 0$
- Terminal conditions: $\mathbf{r}(t_f) = \mathbf{r}_f^*, \mathbf{v}(t_f) = \mathbf{v}_f^*$

- 4: Compute the Zero-Effort Miss (ZEM):

$$\mathbf{ZEM} \leftarrow \mathbf{r}_f^* - \mathbf{r}_i - t_{go} \mathbf{v}_i - \frac{1}{2} \mathbf{f}_i t_{go}^2$$

- 5: Compute the Zero-Effort Velocity (ZEV):

$$\mathbf{ZEV} \leftarrow \mathbf{v}_f^* - \mathbf{v}_i - \mathbf{f}_i t_{go}$$

- 6: Calculate the commanded acceleration:

$$\mathbf{u}_i \leftarrow \frac{6k_r}{t_{go}^2} \mathbf{ZEM} - \frac{2k_v}{t_{go}} \mathbf{ZEV}$$

- 7: Enforce acceleration clipping:

$$\mathbf{u} \leftarrow \max(\min(\mathbf{u}_i, u_{\max}), -u_{\max})$$

- 8: Output the optimized parameters k_r, k_v, t_f and the final commanded acceleration \mathbf{u}_i .
-

At the initial time t_0 , the spacecraft's state is given by:

$$\mathbf{r}_0 = \begin{bmatrix} 0 \\ 0 \\ 0.5 \end{bmatrix} \text{ km}, \quad \mathbf{v}_0 = \begin{bmatrix} -0.01 \\ 0 \\ 0 \end{bmatrix} \text{ km/s}$$

This initial state does not correspond to any specific physical scenario (e.g., terminator orbit) and is chosen arbitrarily for the purposes of this study. The terminal conditions are:

$$\mathbf{r}_f = \begin{bmatrix} 0 \\ 0 \\ 0.1222 \end{bmatrix} \text{ km}, \quad \mathbf{v}_f = \begin{bmatrix} 0 \\ 0 \\ 0 \end{bmatrix} \text{ km/s}$$

The target position lies near the surface of the small body, with the soft-landing objective being zero final velocity.

The guidance and simulation parameters used in this study are as follows. The time-to-go (t_{go}) is initialized to $t_{go,0} = 50$ s. The maximum acceleration, and thus the thrust-to-weight ratio of the spacecraft during asteroid proximity operations, is set to $u_{\max} = 0.75 \times 10^{-3}$ km/s². This value is on the upper bound of the ratio even for larger spacecraft, such as the Apollo Lunar Module (LEM). However, this value could be reduced by increasing the time-to-go, allowing for a slower descent. The present setting is intentionally aggressive as this study serves as a scholastic example. The glide-slope angle

constraint is defined as $\theta_{\text{glide}} = 15^\circ$. This value strikes a balance, enabling a near-vertical descent without bringing the spacecraft too close to the surface too early in the trajectory, thereby maintaining a safe descent profile. The simulation timestep is $\Delta t_{\text{sim}} = 1$ s, and the guidance update interval is $\Delta t_{\text{guidance}} = 1$ s. A 1 Hz guidance update rate is reasonable for this example; however, in real flight software, a higher rate of 10–30 Hz is typically preferred.

The numerical integration is performed using MATLAB's `ode113` solver, with absolute and relative tolerances set to 10^{-12} . This multi-step Adams-Basforth-Moulton integrator is well-suited for problems of this nature, balancing computational speed and accuracy. The optimization in the loop employs the Sequential Quadratic Programming (SQP) method implemented in MATLAB's `fmincon`. Sequential Quadratic Programming is an iterative approach for solving constrained nonlinear optimization problems. It can be considered a quasi-Newton method and is applicable to problems where both the objective function and constraints are twice continuously differentiable, though not necessarily convex. SQP solves a series of subproblems that optimize a quadratic approximation of the objective function while satisfying a linearization of the constraints. For unconstrained problems, SQP reduces to Newton's method for finding stationary points of the objective function. To enhance computational speed during each guidance cycle, the optimizer settings are adjusted to allow a maximum of 50 iterations and a constraint tolerance of 10^{-3} . This tolerance is sufficient to respect path constraints, such as the glide-slope requirement, to within the order of a meter. While stricter tolerances may improve accuracy, such modifications would necessitate further optimization of the algorithm for speed.

IV. RESULTS AND ANALYSIS

The performance of the adaptive generalized ZEM/ZEV guidance algorithm was evaluated for the soft landing scenario on 25143 Itokawa. The results include the spacecraft's trajectory, the evolution of commanded acceleration, and the convergence of position and velocity to the desired target. Additionally, the evolution of the adaptive gains k_r and k_v are presented, providing insights into the algorithm's adaptive nature. Figure 1 illustrates the spacecraft's trajectory during the descent phase, visualized in the body-fixed frame of Itokawa. The glide-slope constraint is depicted as a cone originating at the target point on the surface. The spacecraft's path, represented in black, adheres to the glide-slope constraint, demonstrating the effectiveness of the adaptive guidance algorithm. Red vectors indicate the direction of the commanded acceleration throughout the descent. For comparison, Figure 2 shows the trajectory obtained without employing the predictor-corrector scheme. This trajectory, also visualized in the body-fixed frame, highlights deviations from the glide-slope constraint and demonstrates the limitations of the guidance algorithm when corrections are not applied. Figure 3 illustrates the evolution of the commanded acceleration components (u_x, u_y, u_z) over time. The acceleration remains within the specified thrust limits ($\pm u_{\max}$), marked

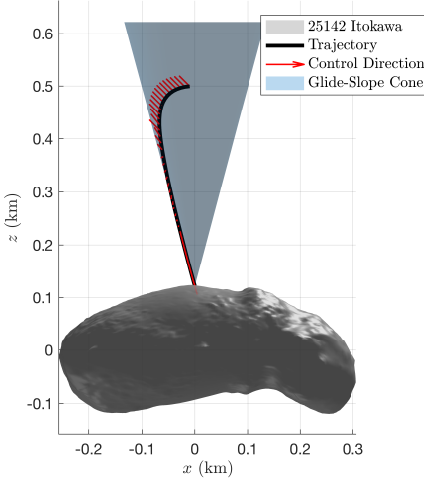


Fig. 1. Spacecraft trajectory with glide-slope constraint shown in the body-fixed frame of 25143 Itokawa.

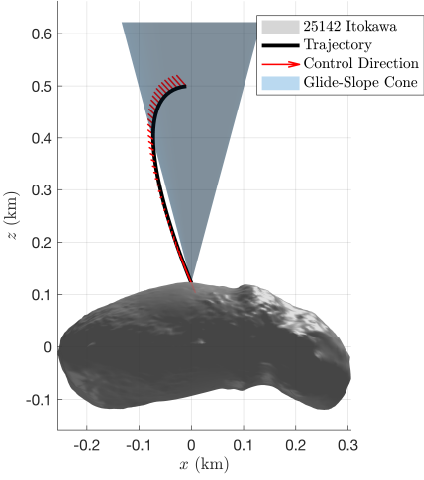


Fig. 2. Spacecraft trajectory without predictor-corrector adjustments, shown in the body-fixed frame of 25143 Itokawa.

by horizontal dashed lines. Within the loop, the algorithm adjusts the guidance parameters to satisfy both path and terminal constraints. However, as previously mentioned, if the maximum number of iterations allowed within the guidance cycle is reached and a solution that fully satisfies the path constraint is not found—primarily impacting the control command, as its order of magnitude is smaller than that of the glide-slope constraint—the commanded control solution is clipped. This implies that, at the specific step, the guidance algorithm does not provide the expected acceleration and must compensate for the clipping in subsequent iterations. While the clipping scheme is effective in ensuring the path constraint on maximum acceleration is respected, it may pose challenges for the glide-slope constraint. Since the guidance law does not provide the expected acceleration during clipping, there is a risk of violating the glide-slope requirement. However, the adaptive and predictive nature of the guidance law at each

step ensures that, even with clipping, both terminal and path constraints are ultimately satisfied. In fact, the maximum value of the glide-slope constraint (which must remain negative) reached during the trajectory was -6.547×10^{-5} , occurring near the very end of the descent.

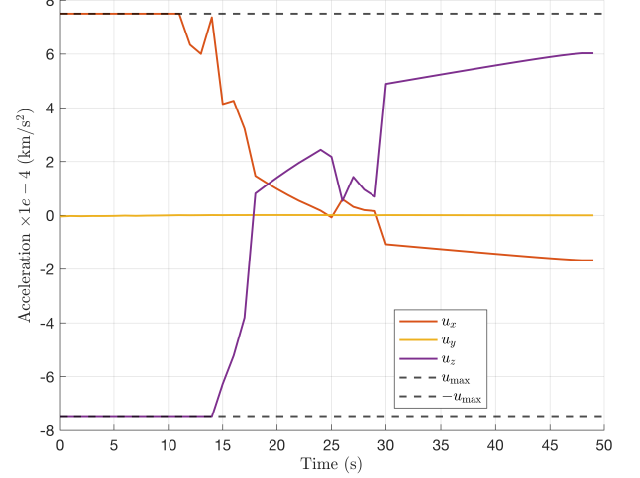


Fig. 3. Time history of commanded acceleration components.

Figure 4 illustrates the convergence of position and velocity over time. The position components (x, y, z) gradually approach the target position (x_f, y_f, z_f), represented by dashed lines. Likewise, the velocity components (v_x, v_y, v_z) successfully reach the desired zero velocity at the target point. This demonstrates the algorithm's capability to meet terminal constraints while respecting the control command upper bound, achieved either through optimization or clipping. The quantitative convergence of the solution to the target state, in addition to the qualitative analysis presented here, will be detailed numerically in the following section using the Monte Carlo analysis.

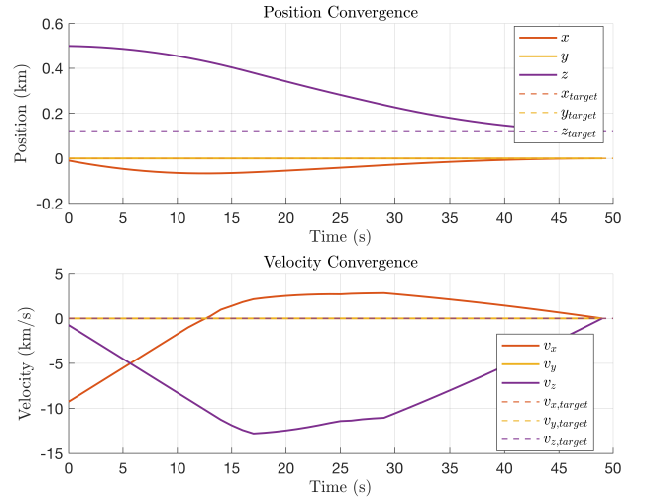


Fig. 4. Convergence of position and velocity components to the target state.

Figure 5 illustrates the time history of the adaptive gains

k_r and k_v . These gains are dynamically adjusted by the optimization process to balance the contributions of ZEM and ZEV in the commanded acceleration. The adaptive nature of these parameters enables the guidance law to handle complex path constraints. The time-to-go is not displayed as it remains effectively constant and shows no noticeable variation during optimization. The results demonstrate the effectiveness of the adaptive generalized ZEM/ZEV algorithm in achieving precise soft landings on small bodies like 25143 Itokawa. The spacecraft successfully adhered to the glide-slope constraint, maintained commanded acceleration within thrust limits, and converged to the desired terminal state. The

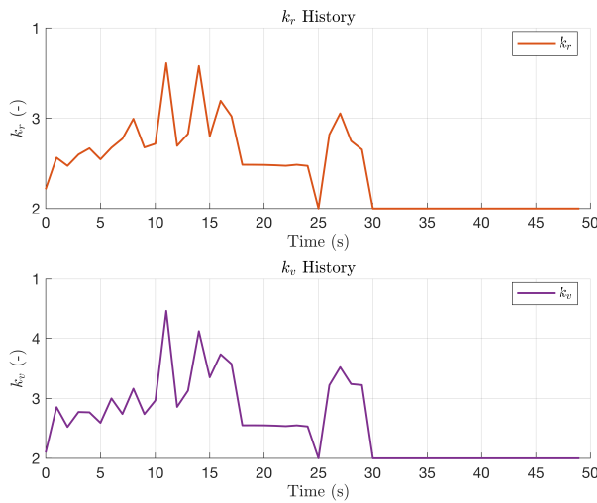


Fig. 5. Evolution of adaptive gains k_r and k_v over time.

guidance law appears ideal: it is parametric, derived from an optimal control problem, straightforward to implement, highly explainable through its mathematical formulation, and capable of imposing arbitrary constraints. However, what is the caveat? In this implementation, the primary bottleneck lies in computational time. Specifically, the CPU time¹ is measured at 2.55 ± 1.99 s, which is far from being ideal (i.e., it is supposed to run here at 1 Hz). This inefficiency stems from the use of `fmincon` within the loop, even when employing a low number of maximum iterations and relatively relaxed tolerances. For a practical implementation, further development is required to mitigate the computational burden. Potential enhancements include creating a custom optimizer, potentially based on a simplified Newton-Raphson method, and leveraging analytical partial derivatives instead of finite differencing. These adjustments could substantially reduce the computational overhead while maintaining the accuracy and flexibility of the guidance law.

V. MONTE CARLO ANALYSIS

To assess the robustness and reliability of the adaptive generalized ZEM/ZEV guidance algorithm, a Monte Carlo

simulation comprising 50 independent runs is conducted. Each run introduced variability through randomly perturbed initial conditions and control inputs, offering statistical insights into the algorithm's performance in achieving a soft landing under diverse uncertainties. The simulation parameters included initial position perturbations modeled as Gaussian noise with a standard deviation of 1% of the nominal position, initial velocity perturbations as Gaussian noise with a standard deviation of 1% of the nominal velocity, and commanded acceleration perturbations as random scaling factors within $\pm 3\%$. All other configurations, including the guidance law scheme, numerical integrator, and optimizer settings, remained consistent with the baseline setup. Figures 6, 7, and 8 summarize the results of the Monte Carlo simulation. Figure 6 illustrates the spacecraft trajectories for all Monte Carlo runs, each adhering to the glide-slope constraint visualized as a cone originating from the target position. This validates the algorithm's robustness in maintaining safe descent paths under perturbations.

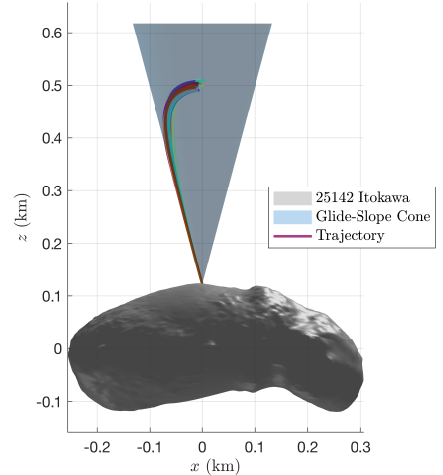


Fig. 6. Spacecraft trajectories for 50 Monte Carlo runs.

The final position and velocity errors for all runs were recorded and statistically analyzed. Figures 7 and 8 present histograms of the position and velocity error norms, respectively. A Gaussian fit was applied to the data, showing that all errors were below 10^{-7} , indicative of excellent precision. The results confirm that the adaptive ZEM/ZEV guidance algorithm consistently achieves high precision in both position and velocity targeting. Despite significant initial perturbations and control variations, all errors remained within acceptable bounds, and the glide-slope constraint was satisfied across all runs. These findings demonstrate the robustness and precision of the proposed adaptive ZEM/ZEV guidance algorithm, making it an excellent candidate for challenging small-body landing missions.

VI. CONCLUSION

This work presented an adaptive generalized ZEM/ZEV guidance algorithm for small-body landing scenarios. The algorithm leverages a parametric guidance law that offers

¹The analysis was conducted on a MacBook Pro equipped with an Apple M3 Pro chip, 12 cores (6 performance and 6 efficiency), and 36 GB of memory.

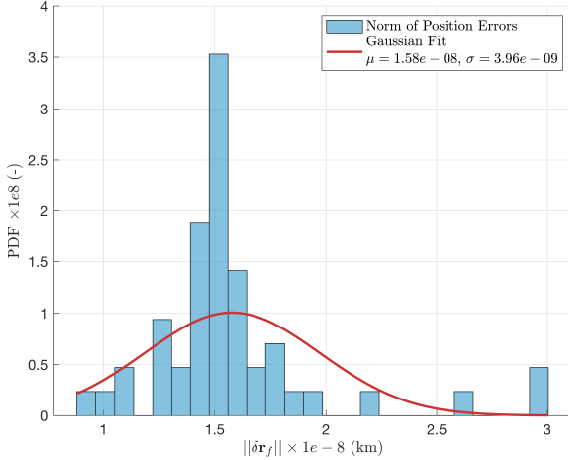


Fig. 7. Histogram of final position error norms with Gaussian fit.

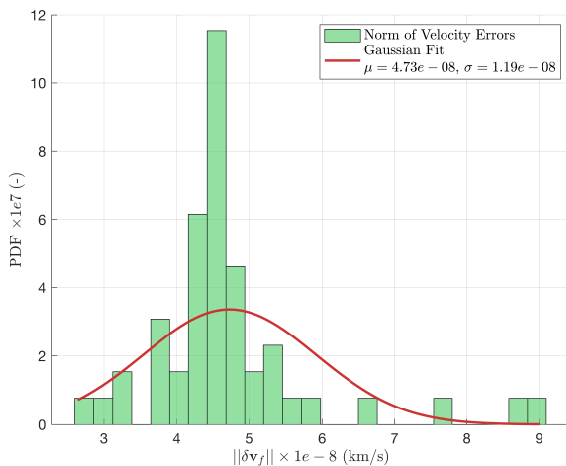


Fig. 8. Histogram of final velocity error norms with Gaussian fit.

flexibility and robustness but loses energy-optimality and cannot inherently handle path constraints under generalized dynamics. To address these limitations, a nonlinear optimizer was incorporated within a predictor-corrector framework. The algorithm successfully managed terminal and path constraints, consistently enforcing the glide-slope constraint and achieving precise terminal position and velocity. Maximum thrust limits were also incorporated, ensuring feasibility. Monte Carlo simulations further validated the algorithm's reliability, demonstrating robust performance under uncertainties in initial conditions and control inputs. However, the reliance on a MATLAB's NLP solver introduces significant computational overhead, limiting real-time onboard implementation. Future work will focus on streamlining the optimization process to overcome this bottleneck. In conclusion, the adaptive ZEM/ZEV guidance algorithm shows strong potential for autonomous landings in small-body missions, offering precision, robustness, and adaptability for challenging space environments.

VII. FUTURE WORK

Future work should focus on enhancing the realism of constraints by introducing lower bounds for control and verifying the feasibility of the control profile through attitude modeling. Additionally, efforts should be directed toward optimizing the algorithm to ensure it can operate at a minimum rate of 1 Hz on a standard laptop, with the ultimate goal of achieving usability on an onboard processor.

VIII. CONTRIBUTIONS AND RELEASE

The sole contributor to this work is the author. All algorithms have been implemented by the author using MATLAB functions such as `fmincon` and `ode113`. The complete project is available in the public repository at the following link: <https://github.com/giovannifereoli/Space-Vehicle-Guidance-Control-2024/tree/main/Project>. The author grants permission for this report to be publicly shared.

REFERENCES

- [1] Clark R. Chapman. The hazard of near-earth asteroid impacts on earth. *Earth and Planetary Science Letters*, 222(1):1–15, 2004. ISSN 0012-821X. doi: <https://doi.org/10.1016/j.epsl.2004.03.004>.
- [2] J.P. Sanchez and C.R. McInnes. Assessment on the feasibility of future shepherding of asteroid resources. *Acta Astronautica*, 73:49–66, 2012. ISSN 0094-5765. doi: <https://doi.org/10.1016/j.actaastro.2011.12.010>.
- [3] Andrew F. Cheng, Andrew S. Rivkin, Patrick Michel, Justin Atchison, Olivier Barnouin, Lance Benner, Nancy L. Chabot, Carolyn Ernst, Eugene G. Fahnestock, Michael Kueppers, Petr Pravec, Emma Rainey, Derek C. Richardson, Angela M. Stickle, and Cristina Thomas. Aida dart asteroid deflection test: Planetary defense and science objectives. *Planetary and Space Science*, 157:104–115, 2018. ISSN 0032-0633. doi: <https://doi.org/10.1016/j.pss.2018.02.015>.
- [4] P. C. Thomas, J. Wm. Parker, L. A. McFadden, C. T. Russell, S. A. Stern, M. V. Sykes, and E. F. Young. Differentiation of the asteroid Ceres as revealed by its shape. *Nature*, 437(7056):224–226, September 2005. ISSN 1476-4687. doi: 10.1038/nature03938.
- [5] Thomas B. McCord and Francesca Zambon. The surface composition of ceres from the dawn mission. *Icarus*, 318:2–13, 2019. ISSN 0019-1035. doi: <https://doi.org/10.1016/j.icarus.2018.03.004>. The Composition of Ceres.
- [6] D. S. Lauretta, S. S. Balram-Knutson, E. Beshore, W. V. Boynton, C. Drouet d'Aubigny, D. N. DellaGiustina, H. L. Enos, D. R. Golish, C. W. Hergenrother, E. S. Howell, C. A. Bennett, E. T. Morton, M. C. Nolan, B. Rizk, H. L. Roper, A. E. Bartels, B. J. Bos, J. P. Dworkin, D. E. Highsmith, D. A. Lorenz, L. F. Lim, R. Mink, M. C. Moreau, J. A. Nuth, D. C. Reuter, A. A. Simon, E. B. Bierhaus, B. H. Bryan, R. Ballouz, O. S. Barnouin, R. P. Binzel, W. F. Bottke, V. E. Hamilton, K. J. Walsh, S. R. Chesley, P. R. Christensen, B. E. Clark, H. C. Connolly, M. K. Crombie, M. G. Daly, J. P.

- Emery, T. J. McCoy, J. W. McMahon, D. J. Scheeres, S. Messenger, K. Nakamura-Messenger, K. Righter, and S. A. Sandford. OSIRIS-REx: Sample Return from Asteroid (101955) Bennu. *Space Science Reviews*, 212(1):925–984, October 2017. ISSN 1572-9672. doi: 10.1007/s11214-017-0405-1.
- [7] Tetsuo Yoshimitsu, Jun’ichiro Kawaguchi, Tatsuaki Hashimoto, Takashi Kubota, Masashi Uo, Hideo Morita, and Kenichi Shirakawa. Hayabusa-final autonomous descent and landing based on target marker tracking. *Acta Astronautica*, 65(5):657–665, 2009. ISSN 0094-5765. doi: <https://doi.org/10.1016/j.actaastro.2009.01.074>.
- [8] Go Ono, Fuyuto Terui, Naoko Ogawa, Shota Kikuchi, Yuya Mimasu, Kent Yoshikawa, Hitoshi Ikeda, Yuto Takei, Seiji Yasuda, Kota Matsushima, Tetsuya Masuda, Takanao Saiki, and Yuichi Tsuda. Gnc strategies and flight results of hayabusa2 first touchdown operation. *Acta Astronautica*, 174:131–147, 2020. ISSN 0094-5765. doi: <https://doi.org/10.1016/j.actaastro.2020.04.029>.
- [9] Stephan Ulamec, Cinzia Fantinati, Michael Maibaum, Koen Geurts, Jens Biele, Sven Jansen, Oliver Küchemann, Barbara Cozzoni, Felix Finke, Valentina Lommatsch, Aurelie Moussi-Soffys, Cedric Delmas, and Laurence O’Rourke. Rosetta lander – landing and operations on comet 67p/churyumov–gerasimenko. *Acta Astronautica*, 125:80–91, 2016. ISSN 0094-5765. doi: <https://doi.org/10.1016/j.actaastro.2015.11.029>. Rosetta and Philae at comet 67P/Churyumov-Gerasimenko.
- [10] Pedro Simplício, Andrés Marcos, Eric Joffre, Mattia Zamaro, and Nuno Silva. Review of guidance techniques for landing on small bodies. *Progress in Aerospace Sciences*, 103:69–83, 2018. ISSN 0376-0421. doi: <https://doi.org/10.1016/j.paerosci.2018.10.005>.
- [11] R. Furfarò and R. D. Wibben. Robustification of a class of guidance algorithms for planetary landing: Theory and applications. In *26th AAS/AIAA Space Flight Mechanics Meeting*. Univelt Inc., 2016.
- [12] Lars Blackmore, Behçet Açıkmeşe, and Daniel P. Scharf. Minimum-landing-error powered-descent guidance for mars landing using convex optimization. *Journal of Guidance, Control, and Dynamics*, 33(4):1161–1171, 2010. doi: 10.2514/1.47202.
- [13] Ping Lu. Propellant-optimal powered descent guidance. *Journal of Guidance, Control, and Dynamics*, 41(4):813–826, 2018. doi: 10.2514/1.G003243.
- [14] Yanning Guo, Matt Hawkins, and Bong Wie. Applications of generalized zero-effort-miss/zero-effort-velocity feedback guidance algorithm. *Journal of Guidance, Control, and Dynamics*, 36(3):810–820, 2013. doi: 10.2514/1.58099.
- [15] Yanning Guo, Matt Hawkins, and Bong Wie. Waypoint-optimized zero-effort-miss/zero-effort-velocity feedback guidance for mars landing. *Journal of Guidance, Control, and Dynamics*, 36(3):799–809, 2013. doi: 10.2514/1.58098.
- [16] Jorge Nocedal and Stephen J. Wright. *Numerical Optimization*. Springer Series in Operations Research and Financial Engineering. Springer, 2nd edition, 2006. ISBN 978-0387303031. doi: 10.1007/978-0-387-40065-5.
- [17] Daniel Scheeres, Steve Broschart, Steve Ostro, and Lance Benner. *The Dynamical Environment About Asteroid 25143 Itokawa, Target of the Hayabusa Mission*. doi: 10.2514/6.2004-4864.